Preferential sorption of radionuclides on different mineral phases typical for host rocks at the site of the future Russian high level waste repository

Vladimir G. Petrov[a,*], Irina E. Vlasova[a], Anastasiya A. Rodionova[a,b], Vasily O. Yapaskurt[c], Vadim V. Korolev[a], Vladislav A. Petrov[d], Valery V. Poluektov[d], Jörg Hammer[e], Stepan N. Kalmykov[a,f]

[a] Department of Chemistry, Lomonosov Moscow State University, Leninskie Gory 1 bld. 3, Moscow, 119991, Russia
[b] V.I. Vernadsky Institute of Geochemistry and Analytical Chemistry of RAS (GEOKHI RAS), Kosygina str. 19, Moscow, 119991, Russia
[c] Department of Geology, Lomonosov Moscow State University, Leninskie Gory 1 bld. 1, Moscow, 119991, Russia
[d] Institute of Geology of Ore Deposits, Petrography, Mineralogy and Geochemistry of RAS (IGEM RAS), Staromonetnyi per. 35, Moscow, 119017, Russia
[e] BGR Geozentrum Hannover, Stilleweg 2, Hannover, 30655, Germany
[f] NRC 'Kurchatov Institute', Akademika Kurchatova pl. 1, Moscow, 123182, Russia

ARTICLE INFO

ABSTRACT

The sorption behaviour of ^{137}Cs, ^{226}Ra, ^{232,238}U, ^{237,239}Np, ^{239,240}Pu, ^{241,243}Am onto rock samples was analysed using image processing of digital autoradiography and scanning electron microscopy results. The rock samples were collected from deep well R12, located within the proposed site of future Russian high level radioactive waste disposal (the exocontact zone of the Nizhnekansky granitoid massif), at depths of 166–476 m. Sorption experiments were performed under conditions similar to those of the disposal near-field (atmospheric conditions, and composition, pH, and Eh of simulated groundwater solutions). The combination of digital autoradiography and scanning electron microscopy allowed the characterisation of the diverse relative sorption properties of different mineral phases of the specific rock samples. The sorption properties of minerals were expressed in terms of relative sorption efficiency.

1. Introduction

The sustainable development of nuclear energy in 21st century will be impossible without solving problems associated with the accumulation of high level radioactive waste (HLW). The safest and the most appropriate method for dealing with HLW is by disposing conditioned HLW in deep weakly permeable geological formations (IAEA, 2011; OECD NEA, 2013). Currently, there are no such repositories operating in the world, but a significant amount of research in this area has been successfully carried out in Sweden, Finland, Switzerland, France, Belgium, Canada, and the USA, among other locations. Different types of geological formations are suitable for safe disposal of HLW (Alexander et al., 2015; McKinley et al., 2007): e.g. crystalline rocks (granites, gneisses) in Finland and Sweden, sedimentary rocks (claystones) in France, and evaporite rocks (salts) in Germany and the USA.

The proposed Russian multibarrier HLW repository project is to be constructed in the Eniseysky area of the exocontact zone of the Nizhnekansky granitoid massif, located near Zheleznogorsk (Krasnoyarsk region) (Jobmann, 2016). In the multibarrier system,

vitrified HLW (mainly alumophosphate, but borosilicate glass is also under consideration) will be placed in stainless steel canisters, which will then be placed underground at a depth of 450–500 m. The canisters will be placed in vertical wells and a compacted bentonite buffer will fill the space between the canister and the host rock wall. The last barrier, according to the IAEA concept, is the host rock, which consists of different mineralogical compositions and is characterised by various parameters of the porous medium. The first stage of construction of the HLW repository (2019–2024) will be the construction of an underground research laboratory. A safety assessment of the future repository requires modelling of the migration of radionuclides in the host rocks, which is partially determined by the sorption properties of rock-forming minerals towards long-lived radionuclides. Sorption of caesium, strontium, radium, plutonium, neptunium, americium, and selenium on crushed rock samples and plates from the Eniseysky area has been studied, but the distribution of radionuclides in mineral phases has been estimated in qualitative terms only (Konevnik et al., 2017a, 2017b; V.G. Petrov et al., 2015b; Rodionova et al., 2019; Vlasova et al., 2016). In these studies, it was shown that radionuclides predominantly

---

*Corresponding author.
E-mail address: vladimir.g.petrov@gmail.com (V.G. Petrov).

sorb onto phyllosilicate minerals and in zones of microbrecciation, chloritization, and sericitization. Plutonium and americium preferably sorbed onto magnetite/hematite, apatite, and calcite.

Typically, sorption studies with rock samples report distribution coefficient values (K_d) that are suitable only for certain samples under certain conditions (e.g. particular pH-Eh values, salinity levels, and temperatures). Complex systems can be modelled as a sum of separated mineral phases or as one overall component with unique properties (Payne et al., 2013). The first approach can be successfully applied if the system contains one or two main phases responsible for sorption, and all components of the mechanical mixture have a small grain size. For crystalline rock samples, this is usually not the case; grain size is typically larger than 0.1 mm, and all components are incorporated into the sample, so it is difficult to distinguish which one of them is responsible for the sorption. In such a case, we suggest an approach which allows determination of the mineral phases with preferential sorption of radionuclides, estimation of their relative contribution to overall sorption, and prediction of the sorption properties of other rock samples. This method uses image processing of digital radiograms of rock samples with sorbed radionuclides, and scanning electron microscopy.

2. Materials and methods

2.1. Rock samples

Five rock samples from five different depths in the exocontact zone of Nizhnekansky granitoid massif, drilled in deep well R12, were collected: (1) 166 m — layered biotite-sillimanite plagiogneiss; (2) 417 m — layered sillimanite-biotite plagiogneiss, plagiogranite-gneiss with garnet and muscovite; (3) 443 m — fine-grained gabbro-diabase with muscovite; (4) 459 m — migmatized quartz-feldspar granite-gneiss with inclusions of chloritized amphibolite; and (5) 476 m — banded-spotted garnet-biotite plagiogneiss with granitized sections of quartz-feldspar-biotite composition (V. A. Petrov et al., 2015a; Vlasova et al., 2016). The chemical compositions of the rock samples, based on X-ray fluorescence data, are provided in Supplementary Information (Tables S-1 and S-2). Based on SiO_2 content and structure, three groups of rocks were distinguished: felsic rocks — sillimanite-containing plagiogneisses (at 166 and 417 m); intermediate rocks — migmatized granite-gneisses and plagiogneisses (at 459 and 476 m); and mafic rocks — gabbro-diabase (in ortho-amphibolite and at 443 m).

2.2. Sorption experiments

The rock samples were cut into sections with a size of 30 × 12 × 8 mm. The two long faces of the sample plates were polished in order to perform radiography analysis. Sorption experiments were carried out at room temperature in plastic vials using simulated groundwater. The simulated groundwater was prepared from an initial hydrocarbonate-calcium solution with mineralisation of 200 mg/L. This was pre-equilibrated with bentonite at a rate of 1 g/L (bentonite from the '10 Khutor' deposit, Khakassia, Russia). The final solution contained 2.4 mg/L Ca^{2+}, 1.9 mg/L Mg^{2+}, 16.9 mg/L Na^+, 6.8 mg/L Al^{3+}, and 19.5 mg/L Si^{+4}. Solutions were prepared such that each contained only one element of interest (^{137}Cs, ^{226}Ra, ^{232,238}U, ^{237,239}Np, ^{239,240}Pu, ^{241,243}Am), the initial concentration of each element was 10^{-9} mol/L, and inactive carriers were not used for any of the radionuclides. For U, Np, Pu, and Am, the mixture of short-lived and long-lived isotopes was used to achieve the desired concentration. The pH values of the solutions were between 7 and 8. In order to avoid co-precipitation of radionuclides on the surface of the rock samples, the polished plates were aligned vertically. Spatial microdistribution of radionuclides on the surface of polished samples was investigated using a digital radiography method, after sorption steady-state was achieved (within 36 h) and samples were rinsed with Milli-Q water and dried. The determination of the mineral phases in the samples was carried out using a

scanning electron microscope with energy dispersive X-ray spectroscopy (SEM-EDX).

2.3. Digital autoradiography method

The distribution of sorbed radionuclides onto polished rock surfaces was investigated by digital autoradiography (DAR) using the Cyclone Storage System (Perkin Elmer). The DAR technique uses storage phosphor screens (imaging plate) (Takahashi, 2002). DAR is a powerful method to quantitatively determine the small-scale distribution of a radiotracer in different solid samples and tissue sections. The method has a high specification in terms of sensitivity, and a linear dynamic range of five orders of magnitude for signal/exposure (Zhang et al., 2008).

A more detailed description of the DAR method is provided in the Supplementary Information section.

2.4. SEM-EDX analysis

The mineral phase composition and morphology of rock samples were studied using a scanning electron microscope with a thermionic tungsten cathode (JSM-6480LV, Jeol, Japan). The chemical composition of rock-forming minerals was analysed using an electron probe method, utilising an energy-dispersive spectrometer (X-Max-50, Oxford Instruments, GB). INCA software (Oxford Instruments, version 21) was used to process the measurement results based on an XPP-correction algorithm. The standards listed in Supplementary Information (Tables S–3) were used to standardise and optimise the characteristic emission line profiles.

Standard measurements and sample analyses were performed under identical conditions: an accelerating voltage of 20 kV; an electron probe current of 10 nA; and a time constant of 5. The data accumulation rate was 12,000–13,000 pulses per second, with a dead time of about 25%. The accumulation time of the spectra in the energy range from 0 to 20 keV with a resolution of 2048 channels was set to 100 s. Feldspar and mica compositions were analysed by scanning areas of 10 μm², which minimises the migration of low-charged cations due to the thermoelectric effect. Compositions of other minerals were measured in the focused probe mode.

2.5. Relative sorption efficiency calculations

The relative sorption efficiency (RSE) was determined using the following relationship:

$$RSE_{i,j} = \frac{I_{i,j}/I_{j,0}}{S_i/S_0}, \tag{1}$$

where $RSE_{i,j}$ is the relative sorption efficiency of mineral phase i towards radionuclide j; $I_{i,j}$ is the intensity of luminescence on the radiogram attributed to radionuclide j sorbed onto mineral phase i; $I_{j,0}$ is the intensity of luminescence on the radiogram attributed to the radionuclide j sorbed onto the whole surface of a rock sample; S_i is the surface area of mineral phase i; and S_0 is the whole surface area of a rock sample.

Thus, the RSE is determined as the ratio of the fraction of sorbed radionuclide attributed to a specific mineral phase to the fraction of rock sample surface area occupied by this mineral phase.

Using digital autoradiography with storage imaging plates, radiograms of rock samples were obtained in the form of black and white images. In previous work (Rodionova et al., 2019), we developed a methodology for the manual treatment of radiograms, which is schematically represented in Fig. 1. This technique is based on the application of ImageJ software, which allows conversion of a black and white radiogram into a pseudo-coloured image consisting of 16 colours. The conversion was done using a lookup table (LUT). This procedure
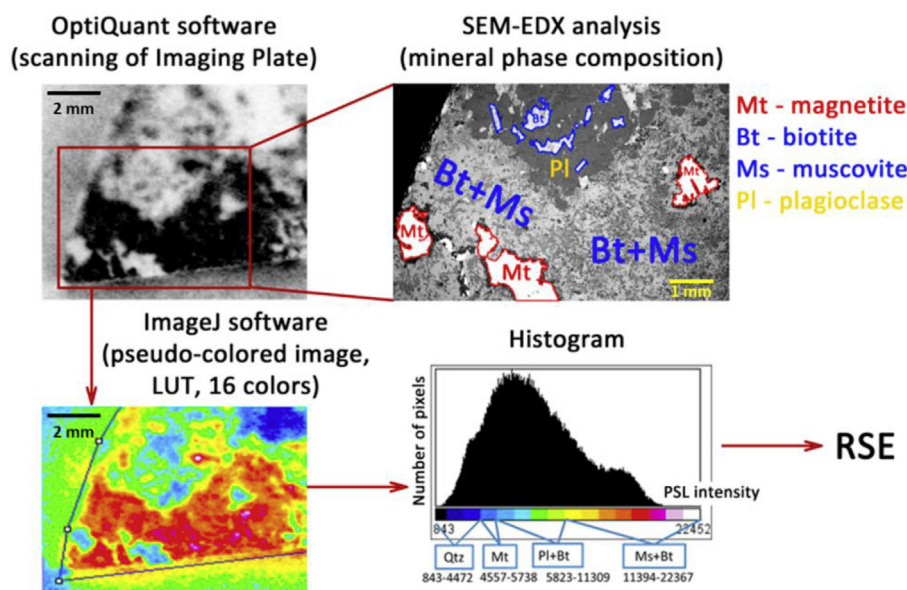
Fig. 1. Calculation scheme for relative sorption efficiency (RSE).

simplified the analysis of radiograms and made it possible to compare the mineral phases of the samples identified using SEM-EDX with the intensities of photostimulated luminescence (PSL) in various areas of the rock sample. The intensity of PSL in each pixel of the radiogram is directly proportional to the activity of the radionuclide. The PSL distribution of the radiogram made it possible to determine the proportion of sorbed radionuclides in different parts of the samples. Finally, a histogram was created showing the surface area of a specific mineral phase (number of pixels) having a particular activity of sorbed radionuclides (PSL intensity).

The main drawback of this procedure is that it requires manual selection of the photostimulated luminescent intensity for specific minerals; often, different minerals have similar PSL values, which makes it almost impossible to correctly differentiate between them. This leads to uncertainty in RSE calculations. In this work, we have applied a different semi-automatic procedure for processing of radiograms and SEM images (see Sections 2.6 and 2.7).

2.6. Radiographic image processing

Radiographic image processing was carried out by applying a median filter with a 3 × 3 kernel to the original radiographic image (an 8-bit grayscale image) three times. The median filter technique is widely used to remove noise, including so-called salt-and-pepper noise (sparsely occurring black and white pixels). This empirically-selected mode allows noise reduction and achieves an appropriate smoothing level.

The original radiographic image has low contrast. To improve the ease of further analysis, we applied Contrast Limited Adaptive Histogram Equalisation (CLAHE) (Pizer et al., 1987). This is a variant of adaptive histogram equalisation with limited contrast amplification. Histograms computed over different regions of the image are used, so local features can be enhanced even in regions which are significantly darker or lighter than most of the image.

2.7. SEM image processing

The main purpose of SEM image processing is the separation of chemical phases based on pixel intensity, i.e. image segmentation. Image segmentation was carried out in two steps, as described below.

The first step was Region Adjacency Graph (RAG) merging (Trémeau and Colantoni, 2000). In this process, the image is divided into small segments, which are considered in further analysis as vertices of an undirected weighted graph. Edge weights depend on the similarity of adjacent nodes (segments). The nodes connected by high-weighted edges are merged until the weights of the remaining edges reach some critically low value.

The second step was K-means clustering (Lloyd, 1982). Since the RAG merging occurs independently, segments related to a single phase may have slightly different intensities. K-means clustering was applied to reduce the amount of segments with different intensities. The algorithm steps are as follows:

1. Select K-cluster centres, where K is expected number of phases.
2. Assign each segment to the nearest cluster centre.
3. Re-calculate the cluster centres by averaging all of the segments in the corresponding cluster.
4. Repeat steps 2 and 3 until convergence.

Image processing was carried out using the scikit-image package (van der Walt et al., 2014). Implementation of K-means clustering was taken from the scikit-learn package (Pedregosa et al., 2012).

3. Results and discussion

In recent work, the manual processing of digital radiograms revealed that the relative sorption efficiency of individual mineral phases has similar values for different rock samples (Rodionova et al., 2019). This indicates the applicability of this approach for estimating the sorption properties of rock samples. However, a major drawback of the methodology is the inability to distinguish mineral phases in many cases. In Tables 1–6, results of the manual and semi-automatic procedures of image processing (digital radiography + scanning electron microscopy) are presented. Compositions in parentheses indicate mixtures of mineral phases for which the contributions in the radiogram could not be separated.

Fig. 2 shows the results of image processing. The converted SEM-image (Fig. 2a) was binarized (Fig. 2b) to create the regions of interest. These regions were further combined (Fig. 2d) using the converted digital radiogram (Fig. 2c). Each region was attributed to a particular mineral phase, as obtained from SEM-EDX data. This combination was subsequently treated as described for manual image processing: the

Table 1
RSE values for caesium sorption. Method 1 is manual treatment, and Method 2 is semi-automatic image processing.

Mineral phases	RSE (Cs) values	
	Method 1	Method 2
quartz	0.6	0.7
(quartz + potassium feldspar)	0.7	**
potassium feldspar	*	0.9
(quartz + plagioclase)	0.8	**
plagioclase	*	1.0
(muscovite + apatite + calcite)	1.4	**
(calcite + apatite)	*	1.4
biotite	1.8	1.4
muscovite	1.8	1.6

*In Method 1, a single mineral phase could not be distinguished and the RSE was defined for a mixture of mineral phases, including the one in question.
**In Method 2, it was possible to separate a mixture of mineral phase into single phases, and the RSE was defined for each individual mineral phase present in the mixture.

Table 2
RSE values for radium sorption. Method 1 is manual treatment, and Method 2 is semi-automatic image processing.

Mineral phases	RSE (Ra) values	
	Method 1	Method 2
magnetite	0.7	0.4
quartz	0.5	0.7
plagioclase	*	0.7
biotite	*	0.8
muscovite	*	1.0
(quartz + chlorite + magnetite)	1.0	**
chlorite	*	1.2
(plagioclase + biotite + magnetite)	1.0	**
(muscovite + biotite)	1.5	1.0

*In Method 1, a single mineral phase could not be distinguished and the RSE was defined for a mixture of mineral phases, including the one in question.
**In Method 2, it was possible to separate a mixture of mineral phase into single phases, and the RSE was defined for each individual mineral phase present in the mixture.

Table 3
RSE values for uranium sorption. Method 1 is manual treatment, and Method 2 is semi-automatic image processing.

Mineral phases	RSE (U) values	
	Method 1	Method 2
quartz	0.5	0.7
(quartz + potassium feldspar)	0.8	**
potassium feldspar	*	1.0
plagioclase	*	1.0
magnetite	*	1.1
muscovite	1.3	1.5
(quartz + potassium feldspar + plagioclase + magnetite)	0.8	**
(plagioclase + magnetite + biotite)	1.2	**
biotite	1.6	1.7

*In Method 1, a single mineral phase could not be distinguished and the RSE was defined for a mixture of mineral phases, including the one in question.
**In Method 2, it was possible to separate a mixture of mineral phase into single phases, and the RSE was defined for each individual mineral phase present in the mixture.

intensity of a particular region was determined from digital radiogram data and the relative surface area of this region was used to calculate the relative sorption efficiency.

This approach allowed us to determine the relative contributions of

Table 4
RSE values for neptunium sorption. Method 1 is manual treatment, and Method 2 is semi-automatic image processing.

Mineral phases	RSE (Np) values	
	Method 1	Method 2
quartz	0.8	0.8
potassium feldspar	*	0.8
(quartz + potassium feldspar + plagioclase)	0.8	**
(plagioclase + biotite)	1.2	**
plagioclase	*	0.9
muscovite	*	1.3
biotite	1.4	1.4
monazite	2.5	2.2

*In Method 1, a single mineral phase could not be distinguished and the RSE was defined for a mixture of mineral phases, including the one in question.
**In Method 2, it was possible to separate a mixture of mineral phase into single phases, and the RSE was defined for each individual mineral phase present in the mixture.

Table 5
RSE values for plutonium sorption. Method 1 is manual treatment, and Method 2 is semi-automatic image processing.

Mineral phases	RSE (Pu) values	
	Method 1	Method 2
quartz	0.8	0.8
plagioclase	0.8	0.9
(quartz + biotite + muscovite)	0.9	**
garnet	*	1.0
muscovite	*	1.2
biotite	1.2	1.1
(biotite + muscovite + garnet)	1.2	**
(magnetite + sillimanite)	1.6	1.6
apatite	*	1.8
chlorite	*	1.9

*In Method 1, a single mineral phase could not be distinguished and the RSE was defined for a mixture of mineral phases, including the one in question.
**In Method 2, it was possible to separate a mixture of mineral phase into single phases, and the RSE was defined for each individual mineral phase present in the mixture.

Table 6
RSE values for americium sorption. Method 1 is manual treatment, and Method 2 is semi-automatic image processing.

Mineral phases	RSE (Am) values	
	Method 1	Method 2
(quartz + muscovite)	0.7	0.9
(quartz + potassium feldspar)	0.8	**
quartz	0.8	0.9
potassium feldspar	*	0.9
garnet	*	0.9
biotite	*	1.0
(biotite + garnet)	1.2	1.0
(magnetite + ilmenite)	1.5	2.0
(calcite + apatite)	1.9	**
magnetite	*	1.4
calcite	*	1.4
apatite	2.0	2.1

*In Method 1, a single mineral phase could not be distinguished and the RSE was defined for a mixture of mineral phases, including the one in question.
**In Method 2, it was possible to separate a mixture of mineral phase into single phases, and the RSE was defined for each individual mineral phase present in the mixture.
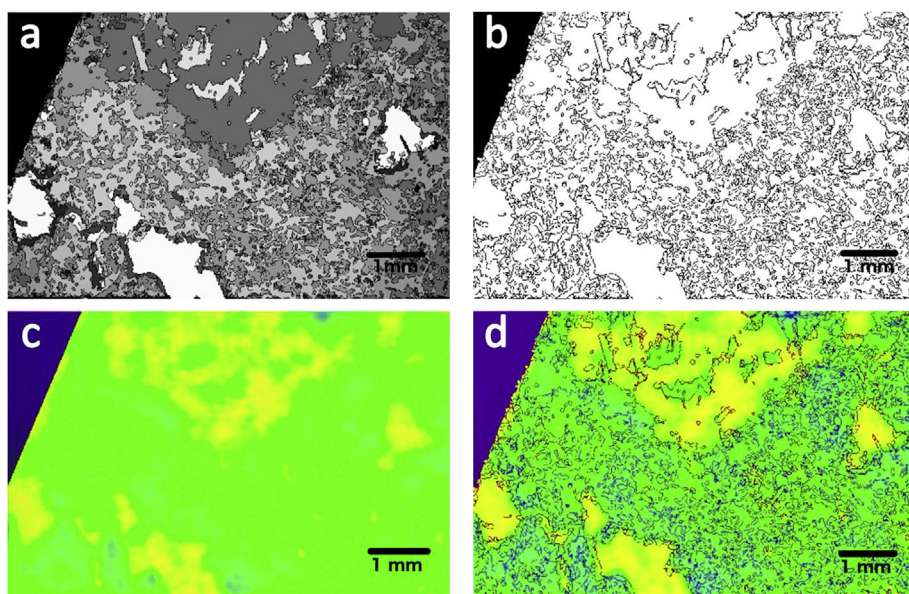
Fig. 2. Semi-automatic image processing for determination of the RSE, considering radium and rock sample 166. a) the converted (clustered) SEM-image of rock sample 166; b) the binarized SEM-image of rock sample 166; c) the converted digital radiogram of radium sorption on rock sample 166; d) the combined result of the binarized SEM-imaged and converted digital radiogram.
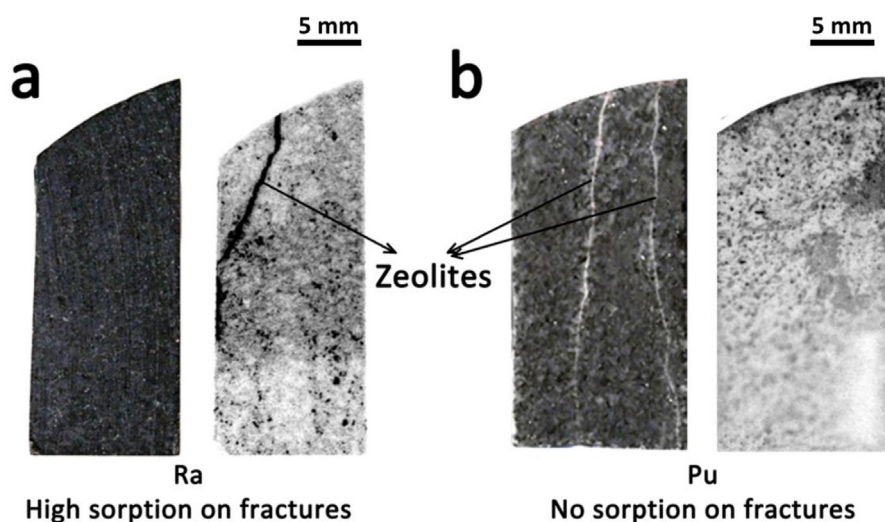

Fig. 3. Comparison of optical images (left) and digital radiograms (right). a) radium sorption on rock sample 443; b) plutonium sorption on rock sample 476.

different mineral phases to the overall radionuclide sorption. In some cases, it was still impossible to distinguish mineral phases due to the DAR resolution of 50 μm, because this is sometimes larger than the mineral grains and because of scattering of radiation in the imaging plate. The manual and semi-automatic approaches showed good agreement when the mineral phases could be easily recognised; this result indicates the convergence of the two methods.

The more precise semi-automatic image processing resulted in the ability to estimate the separate contributions of different mineral phases. RSE values lower than 1 indicate that a particular mineral phase has a lower sorption efficiency towards the radionuclide in question than does the overall rock sample. RSE values higher than 1 indicate that a particular mineral phase has a greater tendency to sorb the radionuclide and can be considered as being mainly responsible for its retention.

In all cases, quartz has a low sorption efficiency. As demonstrated earlier, the most important mineral phases for caesium and radium sorption are cation-exchangeable minerals (biotite and muscovite): RSE (Cs, Ra) values for these minerals were 2–3 times higher than for others. Biotite and muscovite, together with monazite and magnetite, are also responsible for uranium and neptunium sorption. Plutonium and

americium are strongly sorbed onto magnetite, calcite, and apatite mineral phases.

In experiments with separate mineral phases, K_d values can vary by orders of magnitude for different radionuclides and different mineral phases. From the results of the present work, it can be seen that when different mineral phases are simultaneously present in rock, a competitive sorption process takes place. In this case, the difference between different mineral phases is not so profound. Our approach may be useful for modelling radionuclide sorption behaviour in complex systems such as rocks.

In this study, we investigated the sorption of radionuclides on the surface of freshly polished rock samples. We estimated the relative sorption efficiency of different mineral phases towards various radionuclides. But as we observed in some radiograms (Fig. 3), radionuclides can also be effectively sorbed by fracture materials. Thus, it is important to apply the developed technique to evaluate the relative sorption efficiency of fracture-filling minerals.

4. Conclusions

We developed a semi-automatic approach for processing digital

radiogram and scanning electron microscopy images in order to evaluate the relative sorption efficiency of particular mineral phases towards various radionuclides. It was shown that competitive sorption results in smoothing the difference between different mineral phases: e.g. the difference in RSE values for quartz and other minerals, including apatite, magnetite, is only 2 to 3 times, rather than orders of magnitude, as seen in experiments looking at separate mineral phases. The RSE determination made it possible to establish the contribution of each individual mineral to the sorption of a radionuclide in the presence of a particular host rock. We consider this approach to be the next step in understanding the sorption properties of rocks, after sorption experiments with bulk samples, on one hand, and experiments with individual minerals, on the other hand. From the defined RSE values and the known composition of host rock, it will be possible to estimate the overall distribution coefficients. Moreover, the proposed approach makes it possible to estimate the contribution of fracture-filling minerals, which could possibly be the main routes of migration of radionuclides.

We also would like to ask researchers in this field to send us their radiography data (preferably with SEM data) for analysis using the developed approach. This will provide more information based on their data, and will enable us to add to our statistical evaluation in order to obtain more precise determinations of RSE values for different mineral phases and radionuclides.

Acknowledgements

Appendix A. Supplementary data

Supplementary data to this article can be found online at https://doi.org/10.1016/j.apgeochem.2018.11.007.

References

Alexander, W.R., Reijonen, H.M., McKinley, I.G., 2015. Natural analogues: studies of geological processes relevant to radioactive waste disposal in deep geological repositories. Swiss J. Geosci. 108, 75–100. https://doi.org/10.1007/s00015-015-0187-y.

IAEA, 2011. IAEA Safety Standards Geological Disposal Facilities for Radioactive Waste SSG-14 124.

Jobmann, M. (Ed.), 2016. Site-specific Evaluation of Safety Issues for High-level Waste Disposal in Crystalline Rocks. Final Report (URSEL). TEC-28-2015-AB, pp. 181.

Konevnik, Y.V., Zakharova, E.V., Martynov, K.V., Andryushchenko, N.D., Proshin, I.M., 2017a. Influence of temperature on the sorption properties of rocks from the Nizhnekansky massif. Radiochemistry 59, 313–319. https://doi.org/10.1134/S106636221703016X.

Konevnik, Y.V., Zakharova, E.V., Martynov, K.V., Shiryaev, A.A., 2017b. Influence of temperature on the speciation of radionuclides sorbed onto rocks from the Nizhnekansky massif. Radiochemistry 59, 320–325. https://doi.org/10.1134/S1066362217020171.

Lloyd, S., 1982. Least squares quantization in PCM. IEEE Trans. Inf. Theor. 28, 129–137. https://doi.org/10.1109/TIT.1982.1056489.

McKinley, I.G., Russell Alexander, W., Blaser, P.C., 2007. Development of geological disposal concepts. Radioact. Environ. 9, 41–76. https://doi.org/10.1016/S1569-4860(06)09003-6.

OECD NEA, 2013. The Nature and Purpose of the Post-closure Safety Cases for Geological Repositories.

Payne, T.E., Brendler, V., Ochs, M., Baeyens, B., Brown, P.L., Davis, J.A., Ekberg, C., Kulik, D.A., Lutzenkirchen, J., Missana, T., Tachi, Y., Van Loon, L.R., Altmann, S., 2013. Guidelines for thermodynamic sorption modelling in the context of radioactive waste disposal. Environ. Model. Softw. 42, 143–156. https://doi.org/10.1016/j.envsoft.2013.01.002.

Pedregosa, F., Varoquaux, G., Gramfort, A., Michel, V., Thirion, B., Grisel, O., Blondel, M., Prettenhofer, P., Weiss, R., Dubourg, V., Vanderplas, J., Passos, A., Cournapeau, D., Brucher, M., Perrot, M., Duchesnay, É., 2012. Scikit-learn: machine learning in Python. J. Mach. Learn. Res. 12, 2825–2830. https://doi.org/10.1007/s13398-014-0173-7.2.

Petrov, V.A., Poluektov, V.V., Hammer, J.R., Zulauf, G., 2015a. Analysis of mineralogical and deformation-induced transformations of Nizhnekansky Massif rocks to estimate their retention capacity in geological disposal and isolation of radioactive waste. Gorn. Zh. 67–72. https://doi.org/10.17580/gzh.2015.10.13.

Petrov, V.G., Vlasova, I.E., Kuzmenkova, N.V., Kalmykov, S.N., 2015b. Sorption characteristics of rocks in the Yenisei site of Nizhnekansky granitoid massif. Gorn. Zh. https://doi.org/10.17580/gzh.2015.10.15.

Pizer, S.M., Amburn, E.P., Austin, J.D., Cromartie, R., Geselowitz, A., Greer, T., ter Haar Romeny, B., Zimmerman, J.B., Zuiderveld, K., 1987. Adaptive histogram equalization and its variations. Comput. Vis. Graph Image Process 39, 355–368. https://doi.org/10.1016/S0734-189X(87)80186-X.

Rodionova, A.A., Petrov, V.G., Vlasova, I.E., Yapaskurt, V.O., Petrov, V.A., Poluektov, V.V., Hammer, J., Kalmykov, S.N., 2019. Digital radiography for evaluation of the relative efficiency of radionuclide sorption by various rock minerals. Radiochemistry (in press).

Takahashi, K., 2002. Progress in science and technology on photostimulable BaFX:Eu 2þ (X ¼ Cl; Br, I) and imaging plates. J. Lumin. 100, 307–315. https://doi.org/10.1016/S0022-2313(02)00447-7.

Trémeau, A., Colantoni, P., 2000. Regions adjacency graph applied to color image segmentation. IEEE Trans. Image Process. 9, 735–744. https://doi.org/10.1109/83.841950.

van der Walt, S., Schönberger, J.L., Nunez-Iglesias, J., Boulogne, F., Warner, J.D., Yager, N., Gouillart, E., Yu, T., 2014. scikit-image: image processing in Python. Peer J. 2, e453. https://doi.org/10.7717/peerj.453.

Vlasova, I., Petrov, V., Kuzmenkova, N., Kashtanov, A., Petrov, V., Poluektov, V., Kalmykov, S., Hammer, J., 2016. Sorption of radionuclides on the rocks of the exocontact zone of Nizhnekansky granitoid massif. In: MRS Advances, . https://doi.org/10.1557/adv.2017.190.

Zhang, M., Chen, Q., Li, X.F., O'Donoghue, J., Ruan, S., Zanzonico, P., Ling, C.C., Humm, J.L., 2008. Image deconvolution in digital autoradiography: a preliminary study. Med. Phys. 35, 522–530. https://doi.org/10.1118/1.2828198.